

Quantum-inspired Topographic Stereovision

Fanglin Bao^{1,2,*} and Youfei Xie^{1,2}

¹*Department of Physics, School of Science and Research Center for Industries of the Future, Westlake University, Hangzhou 310030, P. R. China.*

²*Institute of Natural Sciences, Westlake Institute for Advanced Study, Hangzhou 310024, P. R. China.*
(Dated: June 2, 2026)

We challenge the long-unquestioned triangulation in distant stereovision, where shape rather than distance is the relevant observable. Our information-regret analysis reveals that the optimal measurements for absolute distance and distance gradient are unexpectedly different and incompatible. To resolve this observable-measurement mismatch, we introduce stereo regularization to address stereo anisotropies that violate prevailing emitter-number conservation, and propose the topographic interferometer, which exploits cross-detector correlations to probe topography without measuring the distance profile. Our interferometer turns parallaxing paths into Mach-Zehnder arms and incorporates a central path as the local oscillator for balanced homodyne detection, saturating the quantum Fisher information with improved topographic error scaling. Our work enables topographic stereovision of thermal sources beyond the Rayleigh limit, thereby establishing a quantum-inspired framework for heat-assisted detection and ranging in remote sensing and astronomy.

Stereovision by triangulation is a century-tested principle of remote sensing and astronomy, exemplified in stellar parallax, Cherenkov telescope arrays [1], and emerging heat-assisted detection and ranging (HADAR) [2]. Triangulation estimates the target's absolute distance but suffers from quadratic error scaling, $\delta Z \propto Z^2$. In stereovision, however, the more relevant observable is the topography, $\theta = \arctan \partial_X Z$, as illustrated in Fig. 1, which has a further-degraded error scaling particularly in the thermal infrared [3] and long-range regimes with significant ghosting effect [4] and diffraction. This observable-measurement mismatch evokes the long-imagined capability of telescopic vision – probing distant topography without measuring absolute distance [5] – and raises a fundamental question: if shape rather than location is desired, is triangulation still the optimal measurement?

The passive nature of astronomical observation precludes the deployment of active quantum techniques such as quantum radar [6, 7] and quantum LiDAR [8, 9]. Instead, recent advances in quantum metrology [10, 11] have unveiled quantum-inspired sub-Rayleigh imaging of thermal sources that achieves the quantum Cramér-Rao bound for unbiased parameter estimation. Demonstrations through modal imaging (*e.g.*, SPADE [10]) or interferometry [12] (*e.g.*, SLIVER [13] or HOM interference [14]) include super-resolution imaging of point sources with arbitrary brightness [15], 3D location of point sources [16, 17], point number estimation [18, 19], and 2D imaging of extended objects [20–22]. When the light source is discretized in the image plane as a set of point emitters, the prevailing paradigm assumes a conserved number of emitters. By contrast, 3D stereovision of extended objects inherently involves multi-detector measurements with angular anisotropy that violates emitter-number conservation.

Here, we introduce stereo regularization to address un-

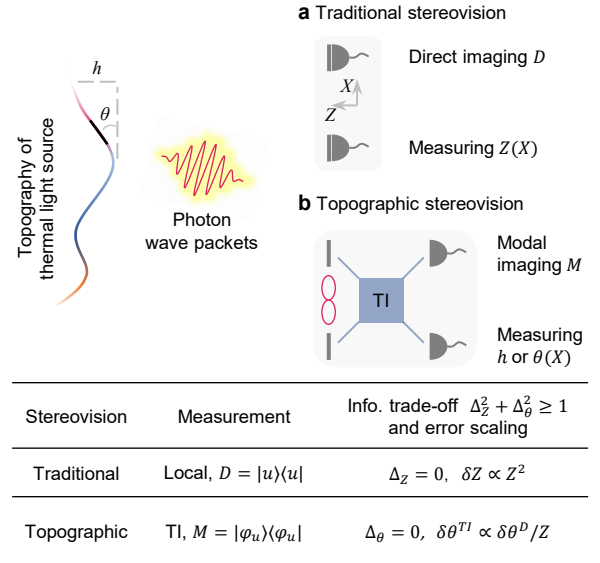


FIG. 1. Quantum-inspired topographic stereovision with topographic interferometer (TI, see Fig. 2). Cross-detector correlations encode unique topographic information beyond triangulation, trading distance precision for improved topographic error scaling. Δ : information regret. u : image plane coordinate. φ_u : modal profile.

controlled anisotropy and identify the unique information associated with emitter-number variations that is accessible only through cross-detector correlations. We propose the topographic interferometer (Fig. 2) with optimal positive-operator valued measures (POVMs) to trade distance precision for improved topographic error scaling.

Considering a stereovision problem in the X - Z plane (Fig. 2), without loss of generality. The thermal source has an unknown one-dimensional object profile (X_r, Z_r) with brightness distribution B_r , where r is the path coordinate along the profile. The interferometer is centered

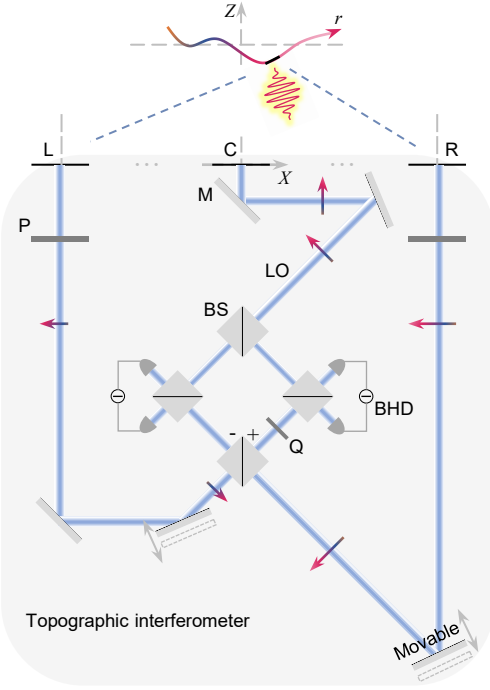


FIG. 2. Topographic interferometer. A thermal photon emitted by the light source (black line segment) propagates (dashed blue line) to the apparatus and is in a superposition across stereo spatial modes (L: left, R: right), which are fed into the bottom beam splitter (BS) for interference. This process resembles a Mach-Zehnder interferometer, in which the contrast between two spatial modes encodes the topography of the thermal light source. We introduce a central spatial mode (C) as the local oscillator (LO) for balanced homodyne detection (BHD) to fully extract the topographic information. M: mirror. P: variable phase retarder. Q: quarter-wave phase retarder. Arrows with varying lengths: virtual images with emitter-number variations. Relay lenses are not shown.

at the origin O with a baseline b , and the apertures are at $X^{(L,C,R)} = (-b/2, 0, b/2)$ and $Z = 0$. In the long-range limit, we are interested in the relative topography h ,

$$\begin{aligned} Z_r &= Z_0 + h_r, & \langle h \rangle &= 0, \\ b, \max |h_r| &\lesssim \max |X_r|, & (1) \\ \varepsilon &= \max |X_r|/Z_0 \ll 1, \end{aligned}$$

where the expectation shall be specified later. Note that h and $\partial_X h$ are deterministically linked in the continuum limit, we refer to topography as either h , $\partial_X h$, or $\theta = \arctan(\partial_X h)$ interchangeably throughout the paper.

Quantum description The incoherent thermal source can be discretized into Q tiny segments with centroid $r_q = (X_q, Z_q)$, tilt angle θ_q , and infinitesimal length dr , $q = 1, 2, \dots, Q$. In the long-range and weak-source limits where the received mean photon number $\epsilon \sim \max |X(r)|^2/Z_0^2 = \varepsilon^2 \ll 1$, the optical field with given polarization and frequency entering the interfer-

ometer has an expansion (see Supplementary Materials),

$$\rho = (1 - \epsilon)\rho_0 + \epsilon\rho_1 + \mathcal{O}(\epsilon^2). \quad (2)$$

Let u denote the image-plane coordinate, $|0\rangle = \otimes_u |0\rangle_u$ the joint vacuum state, and $|u\rangle = a_u^\dagger |0\rangle$ the state with one photon in the spatial mode u . We have $\rho_0 = |0\rangle\langle 0|$, and $\rho_1 = \sum_q I_q |\Psi_q\rangle\langle \Psi_q|$, where

$$|\Psi_q\rangle = \sqrt{\eta_q^L} e^{i\phi_q} |\psi_q^L\rangle + \sqrt{\eta_q^C} |\psi_q^C\rangle + \sqrt{\eta_q^R} e^{-i\phi_q} |\psi_q^R\rangle. \quad (3)$$

Here, $|\psi_q^i\rangle = \sum_{u \in i} S_{uq} / \sqrt{\eta_q^i} |u\rangle$ is the single-photon state of the i -th detector mode ($i = L, C, R$), S_{uq} is the scattering matrix describing the linear but dissipative propagation from source mode q to image mode u , and $\eta_q^i = \sum_{u \in i} |S_{uq}|^2$ is each detector's efficiency with $\eta_q = \sum_i \eta_q^i \leq 1$. Typically, $\eta_q^i \propto A^i \cdot dx^i/dr$ encodes the effective aperture A^i and the image length dx^i of the source segment. The unnormalized intensity distribution $I_q = \epsilon_q^o/\epsilon = \epsilon_q^o/\sum_q \epsilon_q^o \eta_q$ is related to the classical brightness B_r through the emitted mean photon number $\epsilon_q^o = B(r_q)dr \cdot \tau/\hbar\omega$, where τ is the coherence time, \hbar the reduced Planck constant, and ω the frequency. The phase contrast among stereo detectors is $\phi_q = \omega b X_q / 2c Z_q$, c being the speed of light, and we have assumed that the phase is uniform within each detector, *i.e.*, $\omega\sqrt{A^i} X_q / c Z_q \ll 1$.

The optical field acquires propagated coherence in Eq. (3), as in the weak-source limit the thermal state ρ [second-order coherence $g^2(0) = 2$] becomes a single-photon state ρ_1 [$g^2(0) = 0$] by neglecting multi-photon events, *e.g.*, through post selection or by restricting the number of temporal modes (or measurements) T to be $1/\epsilon \ll T \ll 1/\epsilon^2$. If we focus on the stereo arms and denote $|\psi_q^L\rangle = |10\rangle$, $|\psi_q^R\rangle = |01\rangle$ (ignoring coefficient difference), the single-photon wave packet is in a superposition across two detector modes, which can be formally described as a Bell state of maximal qumode entanglement [23], implying that local measurement on each detector such as triangulation might be non-optimal.

Stereo regularization Traditional triangulation estimates image centroids on each detector, $x_q^i = -f(X_q - X^i)/Z_q$, and infers distance through stereo centroid-matching (finding $q' = q$), with disparity $d = x_q^R - x_{q'}^L = bf/Z$. The resulting distance error scales quadratically, $\delta Z = \delta d \cdot Z^2/bf$. Here, f is the focal length. In the thermal-infrared, however, low-contrast self-emission dominates over high-contrast ambient scattering, producing the ghosting effect [4]. Moreover, the longer wavelength ($10 \mu\text{m}$ versus $0.5 \mu\text{m}$ in the visible) exacerbates diffraction and degrades resolution, driving long-range stereo matching deep into the sub-Rayleigh regime. Together, these effects yield large disparity errors δd (from inaccurate q'), making thermal ranging extremely challenging. Emerging HADAR mitigates ghost-

ing by spectral resolution but remains constrained by diffraction-limited resolution [2].

In adopting quantum-inspired imaging for stereovision, two unique features arise: anisotropic projection and anisotropic scattering. Firstly, according to ray optics, the projected image length of the line segment, $dx^i = \frac{f \cdot dr}{Z} [\cos \theta - \sin \theta \cdot \frac{X-X^i}{Z}]$, varies across detectors. When images are discretized into virtual point emitters, one detector sees that the emitter count in other detectors varies, in stark contrast to the prevailing paradigm of emitter-number conservation. Secondly, detectors with different perspectives observe anisotropic scattering from extended objects, depending on the unknown environment and the Bidirectional Reflectance Distribution Function (BRDF). We emphasize that in the long-range limit, the scattering anisotropy can be modeled as a total-intensity correction with coefficient B , consistent with traditional stereovision, which has proven successful so far when using normalized pattern matching instead of absolute-intensity search. These two anisotropies lead to $\sqrt{\eta^L/\eta^C} = \sqrt{A^L dx^L/A^C dx^C} \cdot (1 - B \frac{b}{2Z_0}) \approx (1 - \beta)a_1 + \mathcal{O}(\varepsilon^2)$, $\sqrt{\eta^R/\eta^C} = \sqrt{A^R dx^R/A^C dx^C} \cdot (1 + B \frac{b}{2Z_0}) \approx (1 + \beta)a_2 + \mathcal{O}(\varepsilon^2)$, where $\beta = \frac{b}{2Z_0} \frac{\partial_x h}{2} + B \frac{b}{2Z_0} = \mathcal{O}(\varepsilon)$, $a_1 = \sqrt{A^L/A^C}$, and $a_2 = \sqrt{A^R/A^C}$. To mitigate the uncontrolled scattering, we introduce a stereo regularization that actively sets the effective apertures (*e.g.*, by tilting the apertures) to minimize the integrated absolute difference between the left and right images,

$$\begin{aligned} & \operatorname{argmin}_{a_i} |\operatorname{tr}(\rho^R - \rho^L)| \\ & = \operatorname{argmin}_{a_i} |(a_2^2 - a_1^2) + 2\bar{\beta}(a_2^2 + a_1^2)| + \mathcal{O}(\varepsilon^2), \end{aligned} \quad (4)$$

where $i = \operatorname{argmax}_i \operatorname{tr} \rho^i \in \{L, R\}$, $\rho^i = \sum_q I_q \eta_q^i |\psi_q^i\rangle \langle \psi_q^i|$ is the unnormalized conditioned density operator, and $\bar{\beta} = \langle \beta_q \rangle := \sum_q I_q \eta_q^C \beta_q$. The regularization condition is

$$a_2 = (1 - \bar{\beta})a, \quad a_1 = (1 + \bar{\beta})a, \quad a = \sqrt{a_1 a_2}. \quad (5)$$

Note that stereo regularization does not directly resolve scattering anisotropy, but it enables the extraction of topographic information from unknowns.

Interferometer with optimal POVMs Now we operate the interferometer to illustrate topographic stereovision. Two calibrated movable mirrors move jointly so that their lateral beam shifts have the same magnitude but opposite directions. Denote $x_q = x_q^C$ the central image position, and let x' denote the shifted stereo image position, $x_q^L = x_q^L + \Omega$, $x_q^R = x_q^R - \Omega$, Ω being the untracked lateral translation. We align the image centers by blocking each arm and observing the image at the symmetric port of the bottom beam splitter, and we denote the remaining disparity among stereo detectors as $\delta_q = x_q^R - x_q = x_q - x_q^L$. In the sub-Rayleigh regime, we have $|\delta| = |\langle \delta_q \rangle| \ll \sigma_0$, σ_0 being the width of the point-spread function (PSF). This implies that the interferometer is not gazing at the mean absolute distance

Z_0 but instead at $Z_\delta = Z_0 + \Delta H$ as defined by $\delta = bf/2Z_0 - bf/2Z_\delta$, where $\Delta H = 2\delta \cdot Z_0^2/bf$. Note that the above alignment is intended to roughly establish a gazing reference, not to calibrate the mean distance Z_0 or measure the distance profile Z_r . The residue $h_\delta = h - \Delta H$ is the topography as a perturbation $|h_\delta| \ll Z_\delta$, which requires $|\delta| \ll bf/Z_0$. After all, the remaining disparity becomes $\delta_q = -h_\delta bf/2Z_\delta^2 = \mathcal{O}(\varepsilon)$. Now, we expand functions of x'_q on the beam splitter in terms of x_q to first order. That is, $|\psi(x')\rangle_q^R = |\psi(x)\rangle_q^R + |\psi'(x)\rangle_q^R \delta_q$, and $|\psi(x')\rangle_q^L = |\psi(x)\rangle_q^L - |\psi'(x)\rangle_q^L \delta_q$. Putting together, we have the optical field with explicit topographic dependence,

$$\begin{aligned} |\Psi_q\rangle & = a \sqrt{\eta_q^C} [e^{i\phi_q} (1 - \zeta_q) (|\psi_q^L\rangle - |\psi_q^L\rangle' \delta_q) \\ & \quad + \frac{1}{a} |\psi_q^C\rangle + e^{-i\phi_q} (1 + \zeta_q) (|\psi_q^R\rangle + |\psi_q^R\rangle' \delta_q)], \end{aligned} \quad (6)$$

where $\zeta_q = \beta_q - \bar{\beta}$, with $\langle \zeta_q \rangle = 0$. We specify in Eq. (1) that $\langle h \rangle = \sum_q I_q \eta_q^C h_q = 0$. Note that topographic information in δ is the contribution as if the object is a set of point emitters with fixed counts, while the topographic information in ζ is unique in stereovision that captures fine emitter-number variations.

With cascade unitary transformations of beam splitters, *i.e.*, $|\psi^R\rangle \rightarrow [|\psi^+\rangle + |\psi^-\rangle]/\sqrt{2}$, $|\psi^L\rangle \rightarrow [|\psi^+\rangle - |\psi^-\rangle]/\sqrt{2}$, and so on, the unnormalized conditioned density operator at the balanced output port (top right) is

$$\begin{aligned} \rho^{++} & = \sum_q N_q \{ [\cos^2 \phi_q + (\zeta_q \sin \phi_q + \frac{1}{2a})^2] |\psi_q\rangle \langle \psi_q| \\ & \quad + (\zeta_q + \frac{1}{2a} \sin \phi_q) \delta_q (|\psi_q\rangle \langle \psi_q|)' \\ & \quad + (\sin^2 \phi_q + \zeta_q^2 \cos^2 \phi_q) \delta_q^2 |\psi_q\rangle' \langle \psi_q|' \}, \end{aligned} \quad (7)$$

where $N_q = I_q \eta_q^C a^2$. The bottom right port ρ^{+-} is given by replacing a with $-a$. The effective density operator for the right balanced detection, $\Delta \rho^+ = \rho^{++} - \rho^{+-}$, is

$$\Delta \rho^+ = \sum_q \frac{N_q}{a} \sin \phi_q [2\zeta_q |\psi_q\rangle \langle \psi_q| + \delta_q (|\psi_q\rangle \langle \psi_q|)']. \quad (8)$$

Likewise, the left balanced detection can be obtained by the substitutions: $\sin \phi \rightarrow \cos \phi$, $\cos \phi \rightarrow -\sin \phi$. For a set of POVMs E_n , $\sum_n E_n = I$, the interferometer yields

$$\begin{aligned} \Delta p_n & = \operatorname{tr}(\Delta \rho^\pm E_n) = \int \tilde{h}_x \langle \psi_x | E_n | \psi_x \rangle dx \\ & = \sum_{k=0}^{\infty} \frac{[\partial_x^k \langle \psi_x | E_n | \psi_x \rangle]_{\bar{x}}}{k!} (\tilde{h}_k)^k = \sum_{k=0}^{\infty} G_n^k (\tilde{h}_k)^k, \end{aligned} \quad (9)$$

in the continuum limit, and the dressed topography is

$$\tilde{h}_x = \frac{bf}{2aZ_\delta^2} [\partial_x (N_x e^{i\phi_x}) \cdot h_x + N_x e^{i\phi_x} \cdot \langle \partial_x h_x \rangle], \quad (10)$$

with geometric moments $(\tilde{h}_k)^k = \int \tilde{h}_x(x - \bar{x})^k dx = \mathcal{O}(\varepsilon^k)$, $\bar{x} = \langle x \rangle$. The left and right balanced detections measure the real and imaginary parts, respectively. Note that the intensity distribution $N_x [N(|x - \bar{x}|/\sigma_0 \gg 1) \rightarrow 0]$ can be pre-calibrated experimentally at the central port [22]. Topography can thus be reconstructed by estimating dressed topographic moments \tilde{h}_{2k} and \tilde{h}_{2k+1} , $k = 0, 1, \dots$, whose optimal POVMs achieving the quantum Fisher information

$$K_h = \max_{\{E_n\}} \sum_n (\partial_h p_n)^2 / p_n, \quad p_n = \text{tr}(\rho E_n), \quad (11)$$

satisfy $G_n^j = 0, \forall j < 2k$, and are given by [15, 24]

$$M_{k,k+1}^\pm(u) = |\varphi_{k,k+1}^\pm(u)\rangle\langle\varphi_{k,k+1}^\pm(u)|, \quad (12)$$

where $|\varphi_{k,k+1}^\pm(u)\rangle = [|\varphi_k(u)\rangle \pm |\varphi_{k+1}(u)\rangle] / \sqrt{2}$, and $\varphi_k(u)$ is the k -th Hermite-Gaussian mode, assuming a Gaussian PSF. It can be seen that the above topographic stereovision does not require stereo matching and thus naturally circumvents the ghosting effect without spectral resolution, establishing a quantum-inspired framework for HADAR ranging beyond the Rayleigh limit.

We underscore the key role of the central arm by Eq. (6), where discrete δ (relative distance to the gazing reference) and ζ (tilt angle) are independent. In the limit of $\phi_q \equiv 0$, the output optical field of the bottom beam splitter is, $|\Psi\rangle = a\sqrt{2\eta^C}(|+\rangle + \zeta|-\rangle + \delta|-\rangle') + |\psi\rangle^C / \sqrt{2a}$, where we can see the topographic information lives only in the antisymmetric mode, and so will be the optimal POVMs, $E_n|+\rangle = E_n|\psi\rangle^C = 0$. Consequently, we have $p_n|_{\zeta=0} = \sum_q 2N\delta^2 \langle -|E_n|-\rangle' = \mathcal{O}(\varepsilon^2)$, $\partial_\delta p_n|_{\zeta=0} = 4N\delta \langle -|E_n|-\rangle' = \mathcal{O}(\varepsilon)$, and $K_\delta = \mathcal{O}(1)$. For a single segment, $K_\delta = 8N \max_{\{E_n\}} \sum_n \langle -|E_n|-\rangle' = 2N/\sigma_0^2$, coinciding with the quantum Fisher information for point-separation estimation (δ is half the separation, $2N$ is the total photon number, and hence K differs by a factor of 8) [10]. On the contrary, traditional stereovision relies on local direct imaging, $D_u = |u\rangle\langle u|$, with $p_u^i = \text{tr}(\rho^i D_u) = \mathcal{O}(1)$. The derivative is in the stereo contrast, $\partial_\delta p_u \propto \partial_\delta \text{tr}[(\rho^R - \rho^L)D_u] = \mathcal{O}(\varepsilon)$, due to the fact that $\langle h \rangle = 0$, and its classical Fisher information is $J_\delta^D = \mathcal{O}(\varepsilon^2) \ll K_\delta$. When $\phi_q \neq 0$, however, topographic information is distributed across both symmetric and antisymmetric modes and buried in the phase contrast, rendering the above differential measurements no longer optimal. Nevertheless, we observed that topography is encoded mainly in the real part of the output optical field (after the quarter-wave phase retarder). The optimal measurement is therefore the quadrature POVM with zero phase, implemented via balanced homodyne detection (BHD), with the central mode as the local oscillator. The final classical Fisher information of the interferometer saturates the quantum Fisher information

(single segment),

$$\frac{J_\delta^{\text{TI}}}{K_\delta} = \left[\frac{\sin^2 \phi}{(4a^2 \cos^2 \phi + 1)} + \frac{\cos^2 \phi}{(4a^2 \sin^2 \phi + 1)} \right] \rightarrow 1, \quad (13)$$

in the strong-oscillator limit, $a \ll 1$, for fixed photon budgets on side stereo detectors. This limit can be achieved, *e.g.*, by increasing the bandwidth of the central arm or when considering the propagation loss of stereo arms. Note that even with a weak oscillator, $a \sim 1$, the interferometer can still work near optimal, $J_\delta^{\text{TI}}/K_\delta = \mathcal{O}(1)$.

We argue that the topographic information in ζ associated with emitter-number variation can only be retrieved by cross-detector correlations, not even by adopting SPADE in each stereo detector. Note that $p_n|_{\delta=0} = \sum_q 2N\zeta^2 \langle -|E_n|-\rangle = \mathcal{O}(\varepsilon^2)$, $\partial_\zeta p_n|_{\delta=0} = 4N\zeta \langle -|E_n|-\rangle = \mathcal{O}(\varepsilon)$, and $K_\zeta = \mathcal{O}(1)$. However, to keep ζ -dependence in SPADE, we have $\langle \psi^i | E_{\text{spade}} | \psi^i \rangle_{\bar{x}} \neq 0$, leading to $p^i = \text{tr}(\rho^i E_{\text{spade}}) = \mathcal{O}(1)$. Since $\langle \zeta_q \rangle = 0$, $\partial_\zeta p^i = \mathcal{O}(\varepsilon)$, the classical Fisher information by local SPADE is vanishingly small, $J_\zeta = \mathcal{O}(\varepsilon^2) \ll K_\zeta$. Furthermore, even with SPADE super-resolution imaging (through δ) in each stereo detector, the ghosting effect still hampers accurate stereo matching [4], reflecting the unique advantage of our interferometer.

Scaling law and incompatible measurements

The scaling of quantum Fisher information is $K = \mathcal{O}(\varepsilon^{2k-2})$ for \tilde{h}_{2k} , $K = \mathcal{O}(\varepsilon^{2k})$ for \tilde{h}_{2k+1} , and the classical Fisher information by triangulation is $J = \mathcal{O}(\varepsilon^{2k-2})$ for \tilde{h}_k . Therefore, the ranging error in terms of the k -th order topographic moment has an improvement

$$\delta \tilde{h}_k^{\text{TI}} / \delta \tilde{h}_k^{\text{D}} \propto (b/Z)^{-\lfloor k/2 \rfloor}, \quad (14)$$

where $\lfloor \cdot \rfloor$ is the floor symbol. We illustrate the advantage of our topographic stereovision by detecting a tilted line source (*e.g.*, a planar space debris), with uniform brightness and a linear profile $h_x = f \tan \theta (x - \bar{x}) / Z$, assuming $\phi = 0$. It can be shown that $\tilde{h}_k = 0$ for $k = 0$ and 1, and estimating topography θ involves estimating $\tilde{h}_{k=2} \propto b \tan \theta / Z$, which yields

$$\delta \theta^{\text{TI}} / \delta \theta^{\text{D}} \propto b/Z. \quad (15)$$

This advantage holds for either fixed exposure time or photon budgets, and it strengthens for higher-order-moment estimation.

The interferometer achieves improved topographic precision but is incompatible with distance measurement once the beams are aligned. In fact, the incompatibility has an even more fundamental root in the information trade-off in quantum multiparameter estimation [25],

$$\Delta_Z^2 + \Delta_\theta^2 + 2\sqrt{1 - \tilde{c}^2} \Delta_Z \Delta_\theta \geq \tilde{c}^2, \quad (16)$$

where $\Delta_\mu = \sqrt{(K_\mu - J_\mu)/K_\mu}$ is the information regret describing measurement errors for parameter $\mu = \{Z, \theta\}$,

$\tilde{c} \in [0, 1]$ is the measurement incompatibility,

$$\tilde{c} = \frac{\text{tr}|\sqrt{\rho}[l_Z, l_\theta]\sqrt{\rho}|}{2\sqrt{K_Z K_\theta}}, \quad (17)$$

and l_μ is the symmetric logarithmic derivative (SLD) operator satisfying $l_\mu \rho + \rho l_\mu = 2\partial_\mu \rho$. We illustrate the trade-off with a tiny line segment ($\zeta = 0$), where topographic information is accessible by local measurements (e.g., left detector). We find (see Supplementary Materials)

$$\tilde{c} = \frac{1}{\sqrt{1 + \frac{(dr \cos \theta)^2}{12(X+b/2)^2}}} \rightarrow 1, \quad (18)$$

and hence, $\Delta_Z^2 + \Delta_\theta^2 \geq 1$. While traditional triangulation strives for absolute distance ($\Delta_Z = 0$), topographic stereovision presents an alternative: less distance precision, more topographic information ($\Delta_\theta = 0$).

Our topographic interferometer can be experimentally implemented with configurations similar to a Hanbury-Brown Twiss interferometer (see Supplementary Materials). Our results can be generalized to large photon numbers [11], and large baselines with the assistance of quantum repeaters and entanglement [26, 27]. General BRDF in the short range that deviates from the linear model may require calibration and deserves further study. However, we believe our quantum-inspired topographic stereovision opens new opportunities for passive thermal ranging with applications in remote sensing, astronomy, and non-invasive topographic microscopy.

This work was supported by the National Natural Science Foundation of China. We thank X.-M. Lu for helpful discussions.

* baofanglin@westlake.edu.cn

- [1] <https://www.ctao.org/>.
- [2] F. Bao, X. Wang, S. H. Sureshbabu, G. Sreekumar, L. Yang, V. Aggarwal, V. N. Boddeti, and Z. Jacob, Heat-assisted detection and ranging, *Nature* **619**, 743 (2023).
- [3] R. E. Rivadeneira, A. D. Sappa, B. X. Vintimilla, S. Nathan, P. Kansal, A. Mehri, P. Behjati Ardakani, A. Dalal, A. Akula, D. Sharma, S. Pandey, B. Kumar, J. Yao, R. Wu, K. Feng, N. Li, Y. Zhao, H. Patel, V. Chudasama, K. Prajapati, A. Sarvaiya, K. P. Upla, K. Raja, R. Ramachandra, C. Busch, F. Almasri, T. Vandamme, O. Debeir, N. B. Gutierrez, Q. H. Nguyen, and W. J. Beksi, Thermal image super-resolution challenge - pbvs 2021, in *2021 IEEE/CVF Conference on Computer Vision and Pattern Recognition Workshops (CVPRW)* (2021) pp. 4354–4362.
- [4] W. Treible, P. Saponaro, S. Sorensen, A. Kolagunda, M. O’Neal, B. Phelan, K. Sherbondy, and C. Kambhamettu, Cats: A color and thermal stereo benchmark, in *Proceedings of the IEEE Conference on Computer Vision and Pattern Recognition (CVPR)* (2017); H. Xu, D. Wang, C. Zhao, J. Chen, J. Lin, L. Cao, Y. Zhong, Y. She, and F. Bao, *Universal computational thermal imaging overcoming the ghosting effect* (2026), [arXiv:2604.01542](https://arxiv.org/abs/2604.01542).
- [5] A classic illustration of the concept would be Bond and De La Rue’s experiments in the 1860s, which exploited lunar libration to reveal its mountains and craters in striking depth, even though the Earth–moon distance itself was not measured.
- [6] S. Barzanjeh, S. Guha, C. Weedbrook, D. Vitali, J. H. Shapiro, and S. Pirandola, Microwave quantum illumination, *Phys. Rev. Lett.* **114**, 080503 (2015).
- [7] L. Maccone and C. Ren, Quantum radar, *Phys. Rev. Lett.* **124**, 200503 (2020).
- [8] M. Reichert, R. Di Candia, M. Z. Win, and M. Sanz, Quantum-enhanced doppler lidar, *npj Quantum Information* **8**, 147 (2022).
- [9] G. Qian, X. Xu, S.-A. Zhu, C. Xu, F. Gao, V. V. Yakovlev, X. Liu, S.-Y. Zhu, and D.-W. Wang, Quantum induced coherence light detection and ranging, *Phys. Rev. Lett.* **131**, 033603 (2023).
- [10] M. Tsang, R. Nair, and X.-M. Lu, Quantum theory of superresolution for two incoherent optical point sources, *Phys. Rev. X* **6**, 031033 (2016).
- [11] C. Lupo and S. Pirandola, Ultimate precision bound of quantum and subwavelength imaging, *Phys. Rev. Lett.* **117**, 190802 (2016).
- [12] C. Lupo, Z. Huang, and P. Kok, Quantum limits to incoherent imaging are achieved by linear interferometry, *Phys. Rev. Lett.* **124**, 080503 (2020).
- [13] R. Nair and M. Tsang, Interferometric superlocalization of two incoherent optical point sources, *Opt. Express* **24**, 3684 (2016).
- [14] M. Parniak, S. Borówka, K. Boroszko, W. Wasilewski, K. Banaszek, and R. Demkowicz-Dobrzański, Beating the rayleigh limit using two-photon interference, *Phys. Rev. Lett.* **121**, 250503 (2018).
- [15] S. Zhou and L. Jiang, Modern description of rayleigh’s criterion, *Phys. Rev. A* **99**, 013808 (2019).
- [16] Z. Yu and S. Prasad, Quantum limited superresolution of an incoherent source pair in three dimensions, *Phys. Rev. Lett.* **121**, 180504 (2018).
- [17] Y. Zhou, J. Yang, J. D. Hassett, S. M. H. Rafsanjani, M. Mirhosseini, A. N. Vamivakas, A. N. Jordan, Z. Shi, and R. W. Boyd, Quantum-limited estimation of the axial separation of two incoherent point sources, *Optica* **6**, 534 (2019).
- [18] X.-M. Lu, H. Krovi, R. Nair, S. Guha, and J. H. Shapiro, Quantum-optimal detection of one-versus-two incoherent optical sources with arbitrary separation, *npj Quantum Inf.* **4**, 64 (2018).
- [19] F. Bao, H. Choi, V. Aggarwal, and Z. Jacob, Quantum-accelerated imaging of n stars, *Opt. Lett.* **46**, 3045 (2021).
- [20] M. Tsang, Quantum limit to subdiffraction incoherent optical imaging, *Phys. Rev. A* **99**, 012305 (2019).
- [21] A. A. Pushkina, G. Maltese, J. I. Costa-Filho, P. Patel, and A. I. Lvovsky, Superresolution linear optical imaging in the far field, *Phys. Rev. Lett.* **127**, 253602 (2021).
- [22] Q. Lian, C. Zhang, Q. Tan, J. Zhu, and L. Cao, Incoherent superresolution via diffraction-based hermite-gaussian imaging, *Optica* **13**, 876 (2026).
- [23] X. Jia, C. Zhai, X. Zhu, C. You, Y. Cao, X. Zhang, Y. Zheng, Z. Fu, J. Mao, T. Dai, L. Chang, X. Su, Q. Gong, and J. Wang, Continuous-variable multipartite

- entanglement in an integrated microcomb, *Nature* **639**, 329 (2025).
- [24] J. Frank, A. Duplinskiy, K. Bearne, and A. I. Lvovsky, Passive superresolution imaging of incoherent objects, *Optica* **10**, 1147 (2023).
- [25] X.-M. Lu and X. Wang, Incorporating heisenberg's uncertainty principle into quantum multiparameter estimation, *Phys. Rev. Lett.* **126**, 120503 (2021).
- [26] I. Padilla, A. Sajjad, B. N. Saif, and S. Guha, Superresolution imaging with entanglement-enhanced telescopicity, *Phys. Rev. Lett.* **136**, 010803 (2026).
- [27] P.-J. Stas, Y.-C. Wei, M. Sirotin, Y. Q. Huan, U. Yazlar, F. Abdo Arias, E. Knyazev, G. Baranes, B. Machielse, S. Grandi, D. Riedel, J. Borregaard, H. Park, M. Lončar, A. Suleymanzade, and M. D. Lukin, Entanglement-assisted non-local optical interferometry in a quantum network, *Nature* **651**, 326 (2026).